Ionics (2020) 26:2825–2834
https://doi.org/10.1007/s11581-020-03533-5

ORIGINAL PAPER

Electrochemical properties of pyrolysed graphene/activated carbon composite doped with FeTMPP-Cl as electrode materials

R. M. Ali [1] · O. H. Hassan [2,3] · A. M. M. Ali [3,4] · M. F. M. Taib [3,4] · M. Z. A. Yahya [1]

Received: 4 September 2019 / Revised: 24 February 2020 / Accepted: 10 March 2020 / Published online: 8 April 2020

Abstract

The morphology and electrochemical properties of electrodes made from graphene (Gr)-activated carbon (AC) composite (GrAC) doped with iron(III) tetramethoxyphenylporphyrin chloride (FeTMPP-Cl), hereafter referred to as GrAC-FeTMPP-Cl, are investigated in this study. The properties of the modified electrodes are considerably improved by modifying carbon through the introduction of transition metal catalysts into the hybrid carbon matrix. The hybrid GrAC exhibits superior electrochemical properties than those of materials with single components. Incorporating AC into Gr nanosheets prevents the aggregation of the nanosheets because the AC particles distributed between the Gr layers provide numerous pathways for electron transfer. The addition of FeTMPP-Cl to the electrode material, followed by pyrolysis, enhances the material's electrochemical properties, including fast electron transfer, low charge transfer resistance and high redox current peaks, due to numerous accessible effective surface areas of the electrode. The pyrolysed GrAC-FeTMPP-Cl-modified electrode achieves the highest oxidation current peak of 0.088 mA, with an increment of 10.3% compared with GrAC (0.080 mA) at a scan rate of 20 mVs^{-1} in 5 mM K_3 $[Fe(CN)_6]$/0.1 M KCl electrolyte solution. Results demonstrate the high potential for applications of the pyrolysed GrAC-FeTMPP-Cl/indium tin oxide modified electrode in flexible energy storage devices.

Keywords Graphene · Activated carbon · Electrochemical properties · Catalyst · Electrode · Iron(III) tetramethoxyphenylporphyrin chloride

Introduction

The development of electrochemical energy storage and conversion is essential and has elicited considerable attention worldwide. Electrode materials used in energy storage play a crucial role in electrochemical performance. In the past decade, graphene (Gr) has been widely used as an electrode material because of its large specific surface area (SSA) [1–3], superior electrical conductivity [4] and excellent mechanical strength [5–7]. However, Gr has low packing density [2] and suffers from agglomeration and restacking when it is used as an electrode material [1, 2, 7, 8]. Therefore, controlling the agglomeration and restacking of Gr whilst maintaining its excellent properties has been the primary concern amongst researchers in the past decade. Hybrid carbon materials have been adopted to solve the agglomeration issue and simultaneously achieve desirable volumetric density in electrode materials.

Hybrid carbon materials, such as Gr/carbon nanotubes and Gr/carbon black composites, have been reported to exhibit better electrochemical performance than that of individual materials due to their synergistic effects [2]. A previous study showed that integrating carbon black into the Gr matrix successfully prevented the severe agglomeration of Gr sheets because carbon black functioned as a spacer by partially occupying the spaces in between the Gr sheets and eventually increasing their volumetric density [8]. Carbon black and activated carbon (AC) are widely used as electrode support materials because of their excellent cyclic stability, high SSA, relatively high packing density and low cost [1, 2, 9]. The

✉ M. Z. A. Yahya
mzay@upnm.edu.my

[1] Faculty of Defence Science and Technology, Universiti Pertahanan Nasional Malaysia, 57000 Kuala Lumpur, Malaysia

[2] Faculty of Arts and Design, Universiti Teknologi MARA, 40450 Shah Alam, Malaysia

[3] Ionic Materials and Devices Research Laboratory, Institute of Science, Universiti Teknologi MARA, 40450 Shah Alam, Malaysia

[4] Faculty of Applied Sciences, Universiti Teknologi MARA, 40450 Shah Alam, Malaysia

electrochemical properties of electrode materials can be enhanced by depositing iron(III) tetramethoxyphenylporphyrin chloride (FeTMPP-Cl) catalyst into the hybrid carbon matrix. The thermal treatment of transition metal N_4-macrocyclic complexes (phthalocyanine and porphyrin) changes these compounds into highly active and stable catalysts, increasing the stability and catalytic activity of electrode materials [10–15]. The inner core structure of the N_4-macrocycle remains after pyrolysis and functions as a catalytic centre during electrochemical reaction.

In the current work, pyrolysed GrAC-FeTMPP-Cl/indium tin oxide (ITO) was compared with commercial Gr (Gr/ITO) and hybrid GrAC/ITO. Electrode materials were prepared through simple ultrasonication. Their morphology and structural properties were characterised via scanning electron microscopy (SEM), X-ray diffraction (XRD) and Raman spectroscopy. Meanwhile, their electrochemical properties were characterised via cyclic voltammetry (CV) and electrochemical impedance spectroscopy (EIS). The morphology and electrochemical properties of the electrode materials were discussed in detail to understand the behaviour of hybrid carbon modified with the transition metal N_4-macrocyclic catalyst.

Experimental

Materials

AC powder (Activated charcoal Norit ®, granular form, 1–3 mm); Gr powder (multiple layers, 0.8–1.2 nm); 5, 10, 15, 20-tetrakis (4-methoxyphenyl)-21H, 23H-porphine iron (III) chloride, also referred to as FeTMPP-Cl powder; and all other reagents, including polytetrafluoroethylene (PTFE) binder, acetone and ITO glass, were purchased from Sigma–Aldrich. All chemicals were of analytical grade and used without purification.

Preparation of electrode materials

Gr powder was used as is, whilst granular AC was firstly ground into fine powder before use. GrAC composites with weight ratios of 9:1 and 1:9 were prepared following a previously reported method [16]. Gr and AC powders were firstly dispersed in 200 mL of distilled water through sonication for 5 h at ambient temperature using ultrasonic electronic equipment (Newpower Ultrasonic, Guangzhou Co. Ltd.) to obtain a GrAC suspension. Subsequently, the well-dispersed GrAC aqueous solution was filtered by performing centrifugation two times for 30 min. Lastly, the GrAC powder was dried at 100 °C for 12 h in an oven.

FeTMPP-Cl (25 wt%) was firstly dissolved in acetone, impregnated overnight and ultrasonicated for 30 min. Then, GrAC powder was added to the catalyst solution, and the mixture was subjected to sonication for 1 h to ensure complete suspension and homogenisation. Subsequently, the GrAC-FeTMPP-Cl solution was gradually evaporated on a hot plate at 80 °C. The mixture was dried at 100 °C in an oven to remove the remaining solvent completely.

Pyrolysed samples were obtained by placing GrAC-FeTMPP-Cl powder in a continuous high-purity (99.99%, 5 dm^3 min^{-1}) argon flow furnace at 5 °C min^{-1} heating and cooling rates for heat treatment at 800 °C [17–19]. The temperature was held for 2 h until the designated temperatures were reached as indicated by the furnace sensor.

Electrode modification

The electrodes were prepared using an ITO glass with a projected surface area of 0.25 cm^2. The ITO glass was used as a substrate to coat the prepared working electrode (WE) materials as it offers a wide electrochemical working window along with its promising high electrical conductivity. Prior to modification, the ITO glass was washed successively with acetone and distilled water in an ultrasonic bath and then dried in air. The previously prepared electrode materials and PTFE suspension (60 wt% dispersion in H_2O; 10 μL of binder per mg of GrAC) [20] were dispersed in distilled water using an ultrasonic bath for 20 min. Then, 0.7 μL (1 mg/0.05 mL) of the prepared solutions was cast on the ITO surface and dried at room temperature overnight. The obtained electrodes were labelled AC/ITO, Gr/ITO, GrAC/ITO, GrAC-FeTMPP-Cl-NoHT and GrAC-FeTMPP-Cl-HT800. In this study, the terms NoHT and HT800 are used to represent GrAC-FeTMPP-Cl-NoHT and GrAC-FeTMPP-Cl-HT800, respectively.

Characterisation and electrochemical setup

XRD was performed using BRUKER, XRD D/8. Raman spectroscopy was conducted using a UniRAM-3500, UniRAM (South Korea). Field emission SEM (FESEM) pictures were collected using FESEM LEO 1525 with a GEMINI field emission column. The GEMINI field emission column chamber was attached to an energy-dispersive X-ray (EDX) microanalysis system to qualitatively determine the present elements of the samples. CV and EIS experiments were performed using a Metrohm Autolab 302N potentiostat/galvanostat controlled via NOVA software (V1.11). A standard three-electrode system was used, wherein a modified ITO glass served as the WE, a platinum electrode (Metrohm) as the counter electrode and a silver/silver chloride electrode (Metrohm) as the reference electrode. All measurements were conducted at room temperature (25 ± 1 °C).

Results and discussion

Characterisation of electrode materials

Microstructure of composite electrodes

The FESEM morphology images of Gr (Fig. 1a) show the 3D wavy wrinkles, and the folds of edges are clearly shown in the inset, indicating that several layers of Gr are stacked on top of one another. The images of AC (Fig. 1b) show the structures of the pores and cavities with diameters ranging from 2 to 10 μm. The GrAC composites were prepared in two different ratios (9 Gr:1 AC and 1 AC:9 Gr) to observe the surface morphology differences of the two samples. The surface morphology of GrAC (Fig. 1c, d) with low AC content illustrates that a wrinkled Gr structure is wrapped around the AC particles. Meanwhile, the deposition of high AC content may be disadvantageous because it may lead to the agglomeration of carbon materials, as reported in [21]. The deposition of AC particles in small quantities increases the distance between carbon materials because AC acts as a spacer [22] and arranges them in different directions [23]. The distribution of AC particles on the surface of the Gr layers creates interspaces that provide a large active surface area of GrAC. The GrAC

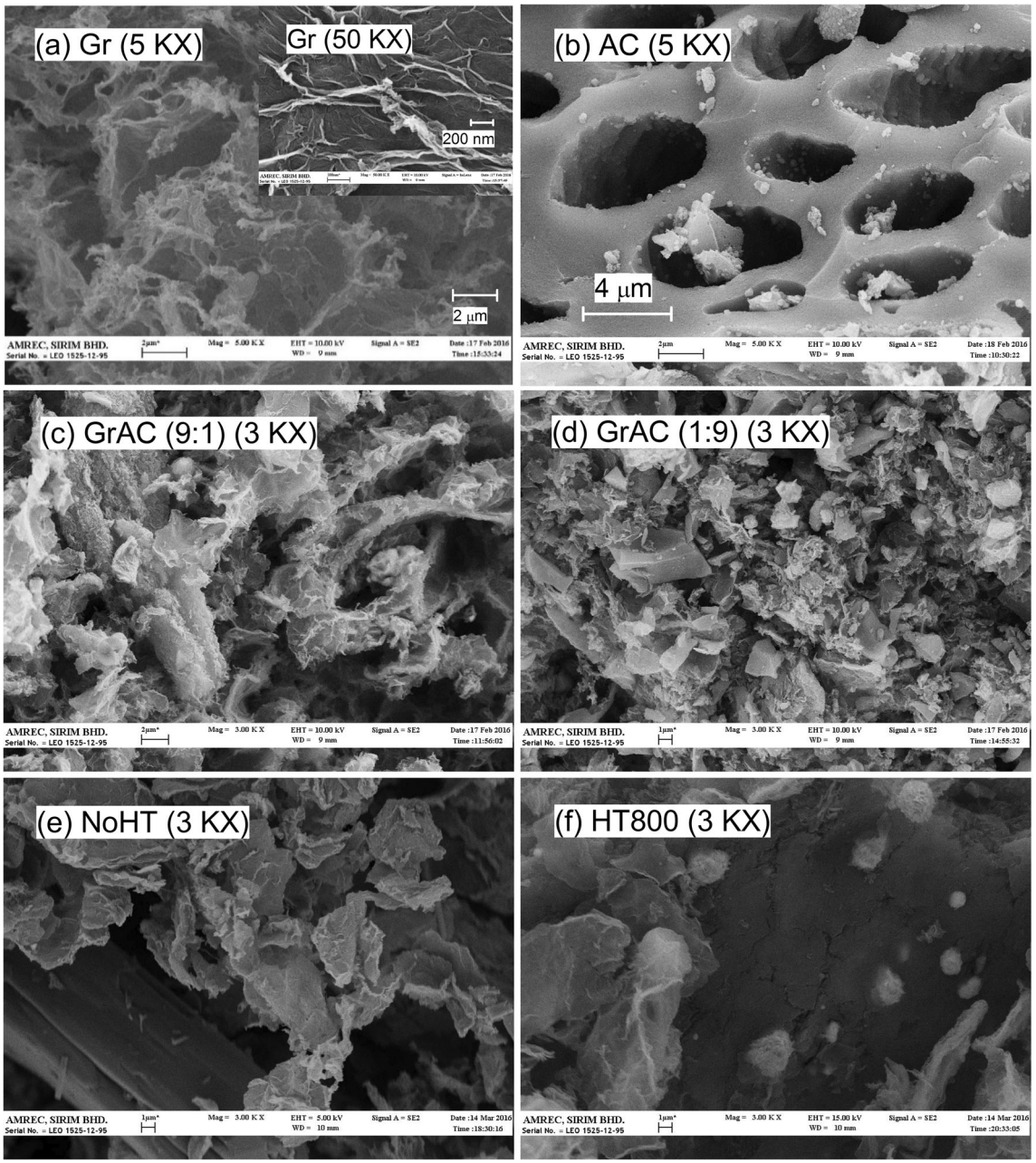

Fig. 1 FESEM images of **a** Gr, **b** AC, **c** GrAC (1:9), **d** GrAC (9:1), **e** NoHT and **f** HT800

with a weight ratio of (9 Gr:1 AC) was used for further characterisation and as electrode materials.

The effect of thermal treatment on surface morphology can be observed on the composite GrAC-FeTMPP-Cl before and after pyrolysis (Fig. 1e, f). The FeTMPP-Cl particles are anchored onto the surface of GrAC. After being pyrolysed in argon atmosphere at high temperatures (800 °C), several catalyst particles are adsorbed into the cracked and porous texture of GrAC and interacted with the functional groups. This finding is in good agreement with that of Qian et al. [24], who reported that the cracked and porous structure allows the reactants to penetrate through the electrode materials.

Chemical composition of electrodes

EDX microanalysis was performed to qualitatively identify the elements present in the samples. The peaks in a spectrum represent element composition. All EDX spectra have carbon and oxygen peaks, indicating their presence in the samples, as shown in Fig. 2.

Phase and structural analysis

XRD was used to evaluate the crystallite nature of the materials. Figure 3 depicts the XRD patterns of commercial AC and Gr, hybrid GrAC, NoHT and HT800. The effects of the FeTMPP-Cl composite on hybrid GrAC and thermal treatment on the GrAC-FeTMPP-Cl composite can be observed from the XRD patterns. The crystallinity of a material was determined on the basis of peak characteristics. That is, high intensity and well-defined peaks indicate the high crystallinity of materials; low-intensity and broad peaks indicate the poor crystallinity of materials resulting from the small and amorphous nature of particles.

In general, carbon and graphite materials are determined by 2θ peaks centred around 26° and 43° [17, 25–34]. The broad and low-intensity peaks at around 25° correspond to the (002) Bragg diffraction of turbostratic (disordered) carbon [28]. Meanwhile, the peak at 43° corresponds to the (100) crystal plane of graphite-type carbon [29–31]. These peaks indicate the presence of a poorly crystallised compound originating from a small particle size and huge amounts of amorphous

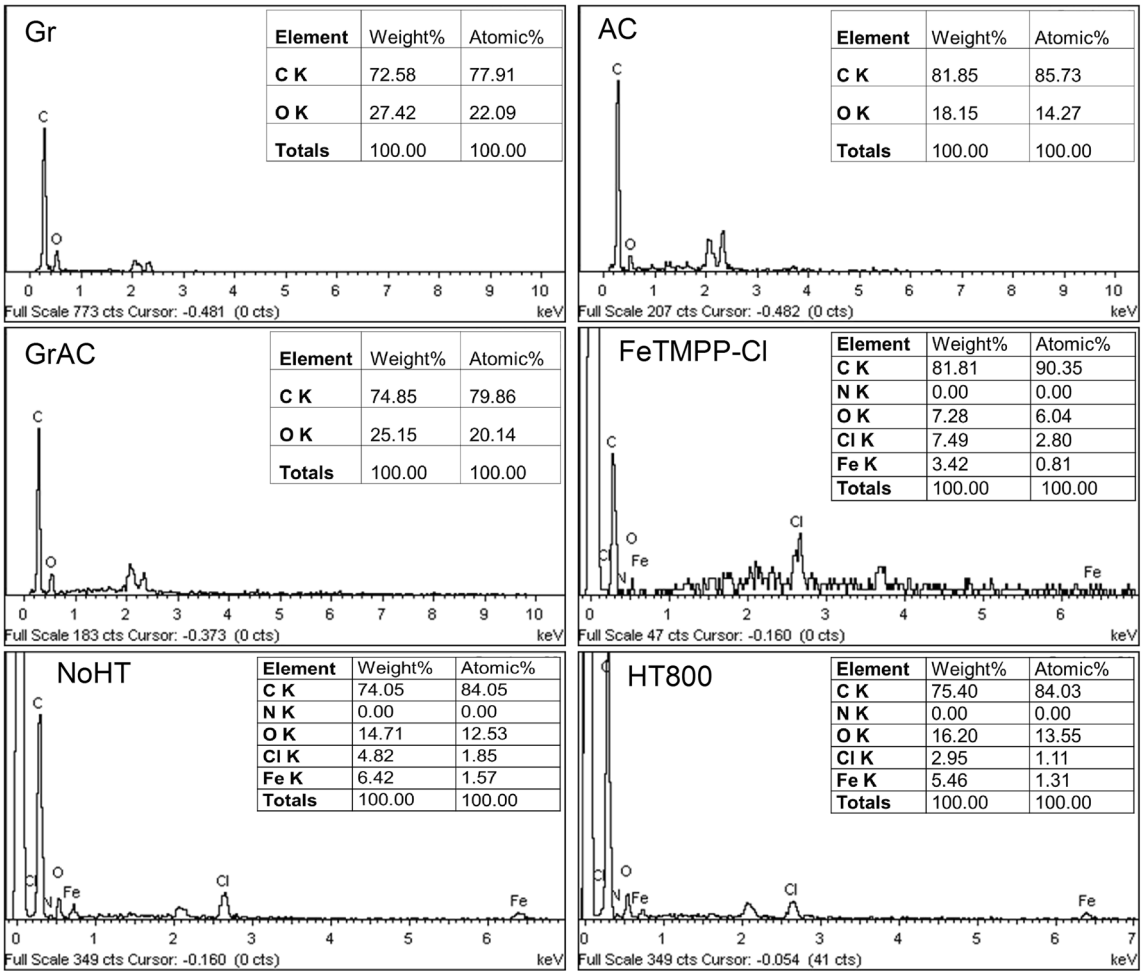

Fig. 2 EDX spectrum and element percentage of electrode materials

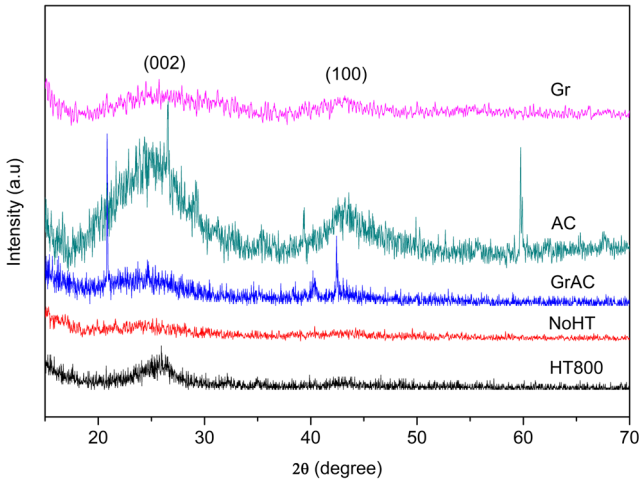

Fig. 3 XRD pattern of electrode materials

carbon nanoparticles [10, 16, 27, 29, 35]. The broadened and decreased peak intensity of GrAC compared with the AC and Gr spectra corresponds to the formation of a new crystal structure that differs from those of AC and Gr. The sharp and well-defined peaks of GrAC appear at 21° and 42°. The peak at 21° is attributed to the orthorhombic lattice of carbon (ICDD No. 00-049-1721). The appearance of minor peaks in the AC pattern may be due to the remaining minerals in the sample. As shown in Fig. 3, the spectrum becomes structureless after the deposition of FeTMPP-Cl, indicating the low degree of graphitisation. The partly restored carbon peak at (002) for HT800 signifies the coexistence of FeTMPP-Cl and hybrid carbon because the inner core structure of the N_4-macrocycle (porphyrin ring) remains after pyrolysis.

The results were confirmed through Raman analysis, as shown in Fig. 4. The Raman spectra of Gr and AC exhibit strong peaks within the range of 1200–1500, 1500–1800 and 2250–2750 cm^{-1} ascribed to the D, G and 2D bands, respectively [3, 7, 8, 17, 29, 30, 33, 36–42]. The two-phonon 2D band is a peak with an asymmetric shape because of various contributions to this peak. Several arguments based on the number of component attributes in the 2D peak of multilayer Gr have been presented. Ferrari [42] claimed that a broad peak consists of four component peaks. Popov [39, 40] proposed the presence of three component peaks. Another study [41] claimed that only two component peaks are involved. Nevertheless, all these studies agreed that a single-layer Gr is supposed to have a pronounced single 2D peak with a full width at half maximum of approximately 25 cm^{-1}, which is considerably more intense than that of the G band. In this case, two components fitted by Lorentzian are used in the Gr sample. This result is consistent with that of a previous report on few-layer Gr and in agreement with the FESEM images. The D band represents the sp^3 defects and disorders in the structures of carbon materials, and the G band corresponds to sp^2 hybridised carbon. The Gr spectrum possesses D and G peaks at 1372 cm^{-1} and 1628 cm^{-1}, respectively. The relative intensity between the two signals, expressed as (I_D/I_G), is frequently used to compare the crystallinity degree of carbon materials, wherein a high (I_D/I_G) value indicates a high degree of disorder in carbon materials [3, 42]. The (I_D/I_G) of hybrid GrAC is slightly lower than that of Gr, implying a better graphitic crystalline structure [30, 33] for this hybrid sample. The relative intensity values of all WE materials are provided in Table 1. The low relative intensity of the HT800 sample can be ascribed to the presence of FeTMPP-Cl nanoparticles between Gr sheets [36]. This observation is in agreement with the XRD results.

Electrochemical study

The electrochemical behaviour of the prepared WEs was evaluated via CV and EIS in 5 mM K_3 [Fe (CN)$_6$] and 0.1 M KCl electrolyte. HT800/ITO was compared with Gr/ITO, hybrid

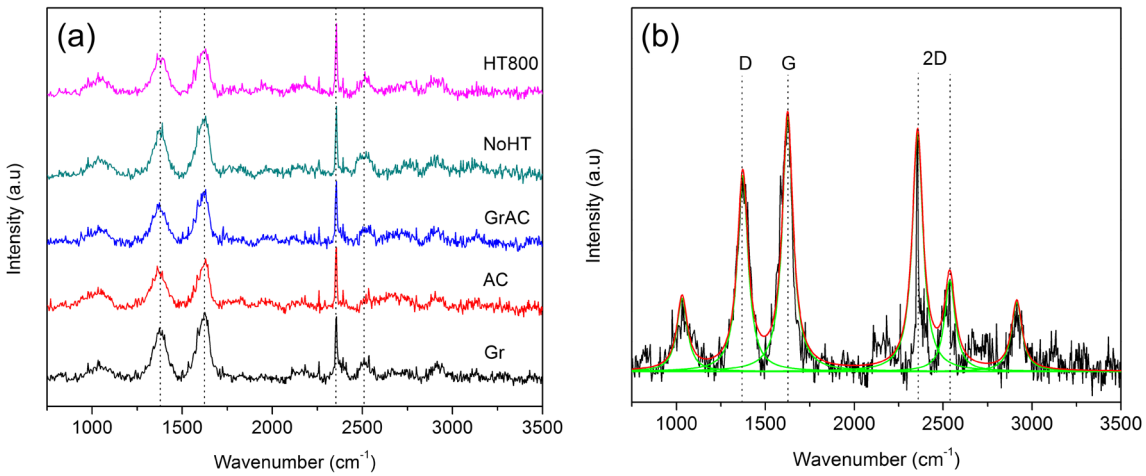

Fig. 4 Raman spectra of **a** electrode materials and **b** Gr analysis peaks (black lines indicate the experimental spectra, and red and green lines denote the stimulated Lorentzian fits and fitted peaks of the components to the experimental spectrum, respectively)

Table 1 The (I_D/I_G) ratios of electrode materials

Sample	(I_D/I_G)
Gr	0.843
AC	0.835
GrAC	0.842
NoHT	0.853
HT800	0.835

GrAC/ITO and NoHT/ITO. All the prepared modified WEs were assessed using a standard three-electrode cell at room temperature. Figure 5 shows the CV curves of the modified WEs at a scan rate of 20 mVs^{-1}. The characteristic parameters of the redox peak are listed in Table 2. The anodic and cathodic peak currents (*I*pa and *I*pc) and the anodic and cathodic peak potentials (*E*pa and *E*pc) were obtained from the CV curves, whilst the ratio of the peak current (*I*pa/*I*pc) and the oxidation and reduction peak potential separation ($\Delta E_p = V\text{pa} - V\text{pc}$) were calculated using the aforementioned parameters. The values of the peak current density ratio were slightly lower than 1, indicating that chemical reaction was involved in the process. As presented in Table 2, the redox peak potentials of Gr appeared at 0.257/0.171 V with ΔE_p determined to be 93 mV. The addition of a small amount of AC into the Gr matrix increased the peak current by 23.5%. The peak current of the HT800 modified electrode increased with the appearance of reduction peaks at 0.259/0.171 V, and ΔE_p was slightly reduced to 88 mV, indicating that the overpotential of the HT800 sample was reduced compared with those of the two other samples. The decreasing ΔE_p value of HT800/ITO compared relative to those of Gr/ITO and GrAC/ITO was correlated with the increasing number of electrons involved in the redox process. Electron transfer at the electrode surface became faster as the difference of peak potentials getting smaller.

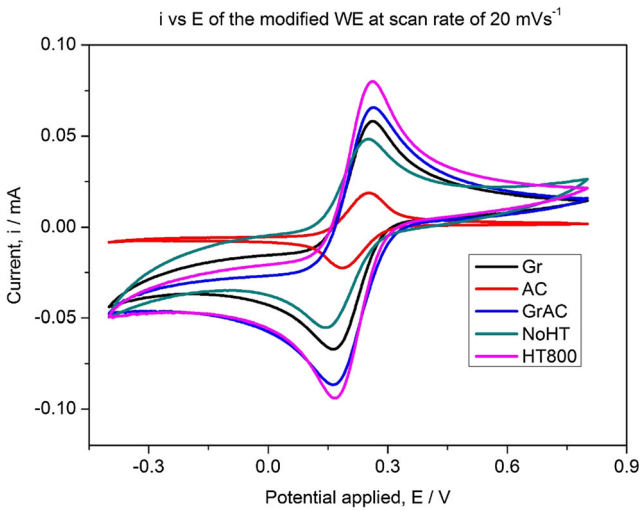

Fig. 5 CVs of modified WEs at scan rate of 20 mVs^{-1}. The CVs were run in 5.0 mM K_3 [Fe $(CN)_6$] solution containing 0.1 M KCl at room temperature (25 ± 1 °C)

The reversibility of the redox reaction can be determined by plotting the square root of the scan rate versus the oxidation peak current (i_{pa} vs. $v^{1/2}$). As shown in the inset of Fig. 6a–d, i_{pa} is proportional to the square root of the scan rate, signifying that the redox processes for all three modified electrodes are reversible. The effective surface area of an electrode can be determined via CV in 5 mM K_3 [Fe $(CN)_6$]/0.1 M KCl solution within the potential range of − 0.4 to + 0.8 V. 5 mM K_3 [Fe $(CN)_6$]/0.1 KCl solution was used as electrolyte to study the oxygen reduction reaction (ORR) of modified electrode since it offers better redox peaks with ITO substrate, thus making it easier to demonstrate the electrode catalytic activities. The oxidation peak current (i_p) was calculated using the Randles–Sevcik equation (Eq. 1).

$$i_p = \left(2.69 \times 10^5\right) n^{\frac{3}{2}} v^{\frac{1}{2}} D^{\frac{1}{2}} AC, \tag{1}$$

where n is the number of transferred electrons ($n = 1$ in the $Fe(CN)_6^{3-}$ redox system), A is the effective surface area of the electrode (cm^2) as given in Eq. 2, C is the molar concentration of $Fe(CN)_6^{3-}$, D is the diffusion coefficient of $Fe(CN)_6^{3-}$ (7.60×10^{-6} cm^2s^{-1}) [43–47] and v is the scan rate (Vs^{-1}). The slope k was obtained by performing linear regression for the i_{pa} versus $v^{1/2}$ plot, which was used to calculate the effective surface area of electrode A, as presented in Table 3.

$$A = k / \left[\left(2.69 \times 10^5\right) n^{\frac{3}{2}} D^{\frac{1}{2}} C\right]. \tag{2}$$

The slopes of the i_{pa} versus $v^{1/2}$ plot for Gr/ITO, GrAC/ITO, NoHT/ITO and HT800/ITO were 4.00×10^{-4}, 4.88×10^{-4}, 2.94×10^{-4} and 5.79×10^{-4}, respectively. The slope of the HT800 electrode was larger than those of the Gr, hybrid GrAC and NoHT electrodes, implying its higher effective surface area, more accessible catalytic sites and improved electron mobility, contributing to its better performance. This phenomenon can be explained by the pyrolysis effect of the transition metal (i.e. FeTMPP-Cl) on the composite GrAC matrix after thermal treatment. The deposition of FeTMPP-Cl into the composite GrAC matrix decreased the oxidation current peak by 45.7%. The heat treatment contributed to the improvement in electron transfer kinetics and mass transfer rate, considerably increasing the oxidation current peak of the pyrolysed electrode material.

Impedance spectra were used to further explore the electrochemical activity of the modified electrodes. Figure 7a–c display the Nyquist plots of the modified electrodes and their equivalent circuit, as shown in the inset of Fig. 7a–c. An equivalent circuit provides information about the interfacial changes caused by the surface modification of electrodes. A

Table 2 CV parameters of modified WEs at scan rate of 20 mVs^{-1}

WE/ ITO	I_{pa} (mA)	I_{pc} (mA)	E_{pa} (mV)	E_{pc} (mV)	I_{pa}/I_{pc}	ΔE_p (mV)
Gr	0.06477	− 0.05867	0.25925	0.16647	− 1.104	93
AC	0.02192	− 0.02024	0.25192	0.18845	− 1.083	63
GrAC	0.07998	− 0.07297	0.26169	0.16891	− 1.096	93
NoHT	0.04341	− 0.04122	0.24704	0.14994	− 1.053	97
HT800	0.08822	− 0.07845	0.25925	0.17136	− 1.125	88

Table 3 Slopes and effective surface area of all modified WEs

WE/ ITO	Slope, k	Effective surface area of electrode, A (cm^2)
Gr	3.9996×10^{-4}	1.08×10^{-4}
GrAC	4.8786×10^{-4}	1.31×10^{-4}
NoHT	2.9361×10^{-4}	0.79×10^{-4}
HT800	5.7912×10^{-4}	1.56×10^{-4}

circuit consists of the ohmic resistance of the electrolyte (R_S), Warburg impedance (Z_W), electron transfer resistance (R_{CT}) and constant phase element (CPE). CPE represents the imperfect double-layer capacitance or interfacial capacitance (C_{DL}). The impedance spectra were analysed on the basis of the equivalent circuit simulated using NOVA software. The Nyquist plots display a depressed semicircle at the high-frequency region and an inclined line approximately 45° in the low-frequency region, except for AC/ITO, which contains only a semicircular part. As shown in the enlarged images in Fig. 7, the intercept at Z' at the very high-frequency region (denoted as R_S) can be observed. In this circuit, R_S represents solution resistance. The semicircular part corresponds to the charge transfer resistance (R_{CT}) at the electrode–electrolyte interface; R_{CT} is equivalent to the diameter of the semicircular part [48, 49]. R_{CT} is expected to be parallel to the double-layer

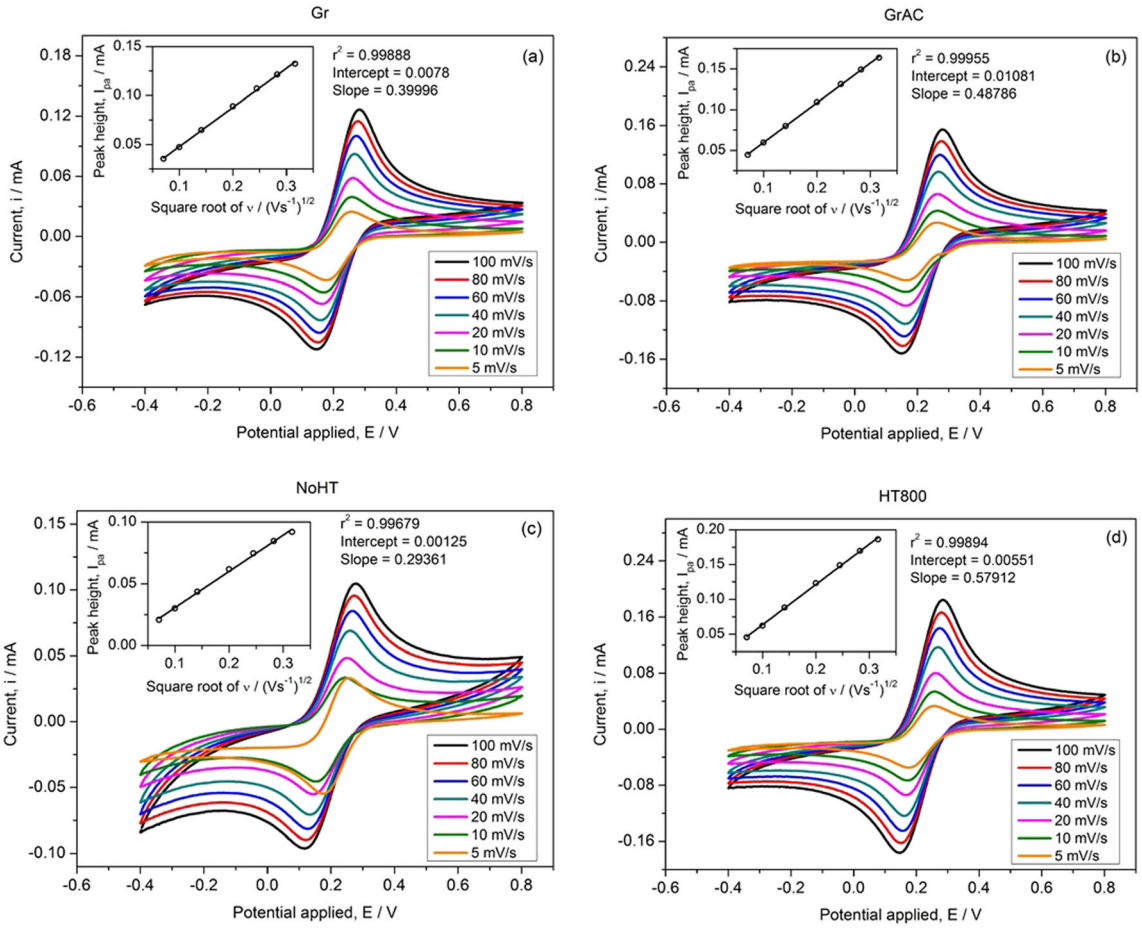

Fig. 6 **a** CVs of modified Gr electrode at different scan rates with the inset of i_{pa} vs. $v^{1/2}$, **b** CVs of modified GrAC electrode at different scan rates with the inset of i_{pa} vs. $v^{1/2}$, **c** CVs of modified NoHT electrode at different scan rates with the inset of i_{pa} vs. $v^{1/2}$ and **d** CVs of modified HT800 electrode at different scan rates with the inset of i_{pa} vs. $v^{1/2}$. All CVs were run in 5.0 mM K_3 [Fe (CN)$_6$] solution containing 0.1 M KCl at room temperature (25 ± 1 °C)

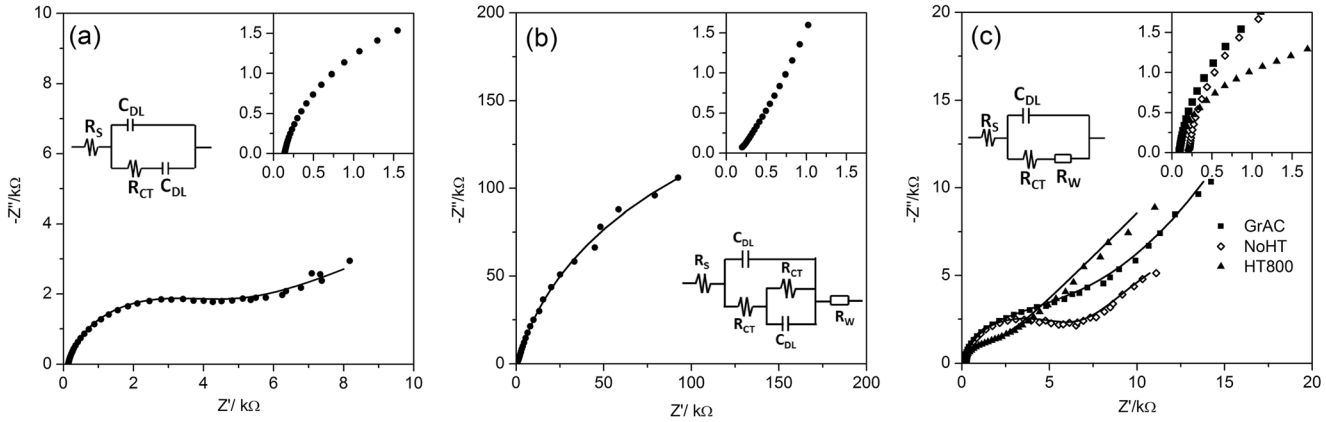

Fig. 7 Nyquist plot of **a** modified Gr electrode with inset of its equivalent circuit and **b** modified AC electrode with inset of its equivalent circuit. All EIS were run in 5.0 mM K_3 [Fe $(CN)_6$] solution containing 0.1 M KCl at room temperature with frequency range of 0.01 Hz to 10 kHz

capacitance (C_{DL}). The inclined part corresponds to the ion diffusion process, which is equivalent to Z_W (line with 45° slope). The lines of the prepared modified electrodes slightly deviated from the ideal vertical line probably because of their rough surface. The rough surface also slightly affects the R_S value. As shown in the Nyquist plots, the diameter of the semicircle for HT800/ITO was smallest compared to other prepared WEs, implying the lowest charge transfer resistance (R_{CT}). The R_{CT} of HT800/ITO is 1.82 k Ω cm^{-1}, followed with Gr/ITO, NoHT/ITO, GrAC/ITO and AC/ITO with R_{CT} value of 2.70 k, 5.21 k, 111 k and 250 k Ω cm^{-1}, respectively. Low R_{CT} accelerates the charge transfer rate of the modified electrode, which led to a better conductivity which enhanced the electrochemical activity of modified WE, while Gr as electrode material has already satisfied this requirement with its low volumetric density. Hybrid GrAC increases the volumetric density and the incorporation of transition metal improved the electronic conductivity hence speeding up the charge transfer rate of the modified electrode. Thus, the thermal treatment of hybrid GrAC doped with FeTMPP catalyst altered this compound into highly stable material whilst possesses great catalytic activity.

Conclusion

In this study, hybrid GrAC and GrAC-FeTMPP-Cl composite materials were successfully prepared using a simple ultrasonication method. The distribution of AC particles on the surface of the Gr layers increased the effective surface area of the electrode material, accelerating electron transfer and reducing resistance during a reversible reaction. The synergistic effect of the Gr sheets and AC increased the redox peaks and effective surface area of the electrode. The thermal treatment of the pyrolysed GrAC-FeTMPP-Cl contributed to the improvement in electron transfer kinetics and effective electrode surface area, considerably increasing the redox peaks of electrode materials.

Acknowledgements The authors would like thank the National Defence University of Malaysia, Universiti Teknologi MARA, AMREC and the Ministry of Education, Malaysia, for the research facilities and the awarded grant.

References

1. Yu S, Li Y, Pan N (2014) KOH activated carbon/graphene nanosheets composites as high performance electrode materials in supercapacitors. RSC Adv 4:48758–48764
2. Zheng C, Zhou X, Cao H, Wang G, Liu Z (2014) Synthesis of porous graphene/activated carbon composite with high packing density and large specific surface area for supercapacitor electrode material. J Power Sources 258:290–296
3. Lei X, Zhang H, Chen Y, Wang W, Ye Y, Zheng C, Deng P, Shi Z (2015) A three-dimensional $LiFePO_4$/carbon nanotubes/graphene composite as a cathode material for lithium-ion batteries with superior high-rate performance. J Alloys Compd 626:280–286
4. Zhai D, Li B, Du H, Gao G, Gan L, He Y, Yang Q, Kang F (2012) The preparation of graphene decorated with manganese dioxide nanoparticles by electrostatic adsorption for use in supercapacitors. Carbon N-Y 50:5034–5043
5. Zhu Y, Murali S, Stoller M-D, Ganesh K-J, Cai W, Feireira P-J, Pirkle A, Wallace R-M, Cyhosz K-A, Thommes M, Su D, Stach E-A, Ruoff R-S (2011) Carbon-based supercapacitors produced by activation of graphene. Science 332:1–20
6. Cui L, Liu Y, He X (2014) Iron(II) tetraaminophthalocyanine functionalized graphene: synthesis, characterization and their application in direct methanol fuel cell. J Electroanal Chem 727:91–98
7. Guo R, Zhao L, Yue W (2015) Assembly of core–shell structured porous carbon–graphene composites as anode materials for lithium-ion batteries. Electrochim Acta 152:338–344
8. Chen Y, Zhang X, Zhang H, Sun X, Zhang D, Ma Y (2012) High-performance supercapacitors based on a graphene–activated carbon composite prepared by chemical activation. RSC Adv 2:7747–7753

9. Yuan A, Zhang Q (2006) A novel hybrid manganese dioxide/activated carbon supercapacitor using lithium hydroxide electrolyte. Electrochem Commun 8:1173–1178
10. Bogdanoff P, Herrmann I, Hilgendorff M, Dorbandt I, Fiechter S, Tributsch H (2004) Probing structural effects of pyrolysed CoTMPP-based electrocatalysts for oxygen reduction via new preparation strategies. J New Mater Electrochem Syst 7:85–92
11. Faubert G, Côté R, Guay D, Dodelet J-P, Dénès G, Bertrandc P (1998) Iron catalysts prepared by high-temperature pyrolysis of tetraphenylporphyrins adsorbed on carbon black for oxygen reduction in polymer electrolyte fuel cells. Electrochim Acta 43:341–353
12. Herrmann I, Kramm U-I, Fiechter S, Bogdanoff P (2009) Oxalate supported pyrolysis of CoTMPP as electrocatalysts for the oxygen reduction reaction. Electrochim Acta 54:4275–4287
13. Zhao F, Harnisch F, Schröder U, Scholz F, Bogdanoff P, Herrmann I (2005) Application of pyrolysed iron(II) phthalocyanine and CoTMPP based oxygen reduction catalysts as cathode materials in microbial fuel cells. Electrochem Commun 7:1405–1410
14. Turk K-K, Kruusenberg I, Mondal J, Rauwel P, Kozlova J, Matisen L, Sammelselg V, Tammeveski K (2015) Oxygen electroreduction on MN4-macrocycle modified graphene/multi-walled carbon nanotube composites. J Electroanal Chem 756:69–76
15. Liang H-W, Brüller S, Dong R, Zhang J, Feng X, Müllen K (2015) Molecular metal–Nx centres in porous carbon for electrocatalytic hydrogen evolution. Nat Commun 6:7992
16. Yan J, Wei T, Shao B, Ma F, Fan Z, Zhang M, Zheng C, Shang Y, Qian W, Wei F (2010) Electrochemical properties of graphene nanosheet/carbon black composites as electrodes for supercapacitors. Carbon N-Y 48:1731–1737
17. Li Zhu A, Wang H, Qu W, Li X, Jong Z, Li H (2010) Low temperature pyrolyzed cobalt tetramethoxy phenylporphyrin catalyst and its applications as an improved catalyst for metal air batteries. J Power Sources 195:5587–5595
18. Cheng S, Liu H, Logan B-E (2006) Power densities using different cathode catalysts (Pt and CoTMPP) and polymer binders (Nafion and PTFE) in single chamber microbial fuel cells. Environ Sci Technol 40:364–369
19. Tyurin V-S, Radyushkina K-A, Levina O-A, Tarasevich M-R (2001) Electrocatalytic properties of a composite based on cobalt porphyrin pyropolymer and Nafion. Russ J Electrochem 37:843–847
20. Wei B, Tokash J-C, Chen G, Hickner M-A, Logan B-E (2012) Development and evaluation of carbon and binder loading in low-cost activated carbon cathodes for air-cathode microbial fuel cells. RSC Adv 2:12751–12758
21. Wang B, Qiu J, Feng H, Sakai E (2015) Preparation of graphene oxide/polypyrrole/multi-walled carbon nanotube composite and its application in supercapacitors. Electrochim Acta 151:230–239
22. Yan J, Wei T, Shao B, Fan Z, Qian W, Zhang M, Wei F (2010) Preparation of a graphene nanosheet/polyaniline composite with high specific capacitance. Carbon N-Y 48:487–493
23. Robat-Sarpoushi M, Nasibi M, Moshrefifar M, Mazloum-Ardakani M, Ahmad Z, Reza Riazi H (2015) Electrochemical investigation of graphene/nanoporous carbon black for supercapacitors. Mater Sci Semicond Process 33:89–93
24. Qian Y, Hu Z, Ge X, Yang S, Peng Y, Kang Z, Liu Z, Lee J-Y, Zhao D (2017) A metal-free ORR/OER bifunctional electrocatalyst derived from metal-organic frameworks for rechargeable Zn-air batteries. Carbon N-Y 111:641–650
25. He X, Lei J, Geng Y, Zhang X, Wu M, Zheng M (2009) Preparation of microporous activated carbon and its electrochemical performance for electric double layer capacitor. J Phys Chem Solids 70:738–744
26. Sui L, Tang S, Chen Y, Dai Z, Huangfu H, Zhu Z, Qin X, Deng Y, Haarberg G-M (2015) An asymmetric supercapacitor with good electrochemical performances based on $Ni(OH)_2$/AC/CNT and AC. Electrochim Acta 182:1159–1165
27. Pouretedal H-R, Sadegh N (2014) Effective removal of amoxicillin, cephalexin, tetracycline and penicillin G from aqueous solutions using activated carbon nanoparticles prepared from vine wood. J Water Process Eng 1:64–73
28. Sun H, Li A, Zhu Z, Liang W, Zhao X, La P, Deng W (2013) Superhydrophobic activated carbon-coated sponges for separation and absorption. ChemSusChem 6:1057–1062
29. Yan J, Fan Z, Wei T, Qian W, Zhang M, Wei F (2010) Fast and reversible surface redox reaction of graphene–MnO_2 composites as supercapacitor electrodes. Carbon N-Y 48:3825–3833
30. Fan Z, Yan J, Zhi L, Zhang Q, Wei T, Feng J, Zhang M, Qian W, Wei F (2010) A three-dimensional carbon nanotube/graphene sandwich and its application as electrode in supercapacitors. Adv Mater 22:3723–3728
31. Fan Z, Yan J, Wei T, Zhi L, Ning G, Li T, Wei F (2011) Asymmetric supercapacitors based on Graphene/MnO_2 and activated carbon nanofiber electrodes with high power and energy density. Adv Funct Mater 21:2366–2375
32. Hwang Y, Kim M, Kim J (2013) Enhancement of thermal and mechanical properties of flexible graphene oxide/carbon nanotube hybrid films though direct covalent bonding. J Mater Sci 48:7011–7021
33. Miao X, Pan K, Pan Q, Zhou W, Wang L, Liao Y, Tian G, Wang G (2013) Highly crystalline graphene/carbon black composite counter electrodes with controllable content: synthesis, characterization and application in dye-sensitized solar cells. Electrochim Acta 96:155–163
34. Hong C, Wang X, Yu H, Wu H, Wang J, Liu A (2018) MnO_2 nanowires-decorated carbon fiber cloth as electrodes for aqueous asymmetric supercapacitor. Funct Mater Lett 11:1850034
35. Yan J, Wei T, Fan Z, Qian W, Zhang M, Shen X, Wei F (2010) Preparation of graphene nanosheet/carbon nanotube/polyaniline composite as electrode material for supercapacitors. J Power Sources 195:3041–3045
36. Jing L-Y, Fu A, Li H, Liu J, Guo P, Wang Y, Zhao X-S (2014) One-step solvothermal preparation of Fe_3O_4/graphene composites at elevated temperature and their application as anode materials for lithium-ion batteries. RSC Adv 4:59981–59989
37. Rahimi R, Zargari S, Yousefi A, Yaghoubi-Berijani M, Ghaffarinejad A, Morsali A (2015) Visible light photocatalytic disinfection of E. coli with TiO_2-graphene nanocomposite sensitized with tetrakis(4-carboxyphenyl)porphyrin. Appl Surf Sci 355:1098–1106
38. Yoo E, Zhou H (2013) Fe phthalocyanine supported by graphene nanosheet as catalyst in Li–air battery with the hybrid electrolyte. J Power Sources 244:429–434
39. Popov V-N (2015) 2D Raman band of single-layer and bilayer graphene. J Phys Conf Ser 682:012013
40. Popov V-N, Lambin P (2012) Theoretical Raman intensity of the G and 2D bands of strained graphene. Carbon N-Y 54:86–93
41. Frank O, Mohr M, Mailtzsch J, Thomsen C, Riaz I, Jalil R, Novoselov K-S, Tsoukleri G, Parthenios J, Papagelis K, Kavan L, Galiotis C (2011) Raman 2D band splitting in graphene, Raman 2D-band split: graphene theory exp. ACS Nano 5:2231–2239
42. Ferrari A-C, Meyer J-C, Scardaci V, Casiraghi C, Lazzeri M, Mauri F, Piscanec S, Jiang D, Novoselov K-S, Roth S, Geim A-K (2006) Raman spectrum of graphene and graphene layers. Phys Rev Lett 97:187401
43. Bishop G-W, Ahiadu B-K, Smith J-L, Patterson J-D (2017) Use of redox probes for characterization of layer-by-layer gold nanoparticle-modified screen-printed carbon electrodes. J Electrochem Soc 164:B23–B28
44. Bard A-J, Faulkner L-R (2001) Electrochemical methods: fundamentals and applications, 2nd edn. John Wiley & Sons

45. Grewal Y-S, Shiddiky M-J-A, Gray S-A, Weigel K-M, Gerard A-C, Trau M (2013) Label-free electrochemical detection of an Entamoeba histolytica antigen using cell-free yeast-scFv probes. Chem Commun 49:1551–1553
46. Stevens N-P-C, Rooney M-B, Bond A-M, Feldberg S-W (2001) A comparison of simulated and experimental voltammograms obtained for the $[Fe(CN)_6]^{3-/4-}$ couple in the absence of added supporting electrolyte at a rotating disk electrode. J Phys Chem A 105:9085–9093
47. Apetrei I-M, Apetrei C (2016) Voltammetric determination of melatonin using a graphene-based sensor in pharmaceutical products. Int J Nanomedicine 11:1859–1866
48. Moghim M-H, Eqra R, Babaiee M, Zarei-Jelyani M, Loghavi M-M (2017) Role of reduced graphene oxide as nano-electrocatalyst in carbon felt electrode of vanadium redox flow battery. J Electroanal Chem 789:67–75
49. Du J, Ma L, Shan D, Fan Y, Zhang L, Wang L, Lu X (2014) An electrochemical sensor based on the three-dimensional functionalized graphene for simultaneous determination of hydroquinone and catechol. J Electroanal Chem 722–723:38–45